Thermal Conductivity of Configurable Two-dimensional Carbon Nanotube Architecture and Strain Modulation

H.F. Zhan[1], G. Zhang[2], J. M. Bell[1] and Y.T. Gu*,[1]

[1]School of Chemistry, Physics and Mechanical Engineering, Queensland University of Technology, 2 George St, Brisbane QLD 4109, Australia

[2]Institute of High Performance Computing, Agency for Science, Technology and Research, 1 Fusionopolis Way 138632, Singapore

***Corresponding Author:** Prof. Yuantong Gu

Mailing Address: School of Chemistry, Physics and Mechanical Engineering,
Queensland University of Technology,
GPO Box 2434, Brisbane, QLD 4001, Australia

Telephones: +61-7-31381009 **Fax:** +61-7-31381469

E-mail: yuantong.gu@qut.edu.au

Abstract

We reported the thermal conductivity of the two-dimensional carbon nanotube (CNT)-based architecture, which can be constructed through welding of single-wall CNTs by electron beam. Using large-scale nonequilibrium molecular dynamics simulations, the thermal conductivity is found to vary with different junction types due to their different phonon scatterings at the junction. The strong length and strain dependence of the thermal conductivity suggests an effective avenue to tune the thermal transport properties of the CNT-based architecture, benefiting the design of nanoscale thermal rectifiers or phonon engineering.

Keywords: thermal conductivity. nanoarchitecture, carbon nanotube, tensile strain

Introduction

Carbonaceous nanomaterials, such as carbon nanotube (CNT) and graphene have attracted huge interests from both scientific and engineering communities due to their outstanding mechanical, electronic, chemical, thermal, and other properties. It has been found that the thermal conductivity of carbon materials can range from ~ 0.01 W/mK in amorphous carbon to above 2000 W/mk,[1] demonstrating an five order allowable tuning ranges for the thermal conductivity. In this regard, a comprehensive understanding of the thermal transport properties of carbonaceous nanomaterials is crucial for the design of next generation of nano-devices. For instance, electronic, optoelectronic and photonic devices demand efficient heat removal so as to maintain their operating performance and long-term reliability. Whereas, the thermoelectric devices, requires materials with strongly suppressed thermal conductivity to ensure a

high figure of merit, $ZT=S^2\sigma T/\kappa$ (here, S is the Seebeck coefficient, T is the temperature, and σ and κ are the electrical and thermal conductivity, respectively).

Recent decades have witnessed an increasing researches aiming to explore the effective avenues to modulate the thermal conductivity of carbonaceous materials. For example, researchers have examined the impacts from the geometry size,[2] structure,[3, 4] and doping/heteroatoms[5] on the thermal properties of graphene. Despite the low dimensional nanomaterials, many attempts have also been made to develop more complex nanostructures basing on graphene and nanotube. For example, Zhu *et al*.[6] reported the synthesisation of seamless 3D carbon nanotube graphene hybrid material. Such pillared-graphene structure is reported with tailorable in-plane and out-of-plane thermal transport properties.[7] Earlier studies reveal that under high temperatures, two single wall CNTs (SWNTs) can be welded by electron beam and resulting X-, Y-, or T-like junctions.[8, 9] Employing these junctions as building blocks, a variety of different 2D or 3D CNT-based nanoarchitectures can be constructed.[10, 11]

To date, several works have been reported on the CNT-based nano-architectures, which have focused on their mechanical properties, such as the bending rigidity and shear stiffness,[12] rupture strain,[13] toughness and stiffness,[14] and their thermal transport properties are still lacking of understanding. In this regard, we conduct such a study to assess the thermal conductivity of 2D CNT-based architectures basing on large-scale molecular dynamics (MD) simulations. It is found that different junction types will endow the associated structures with different thermal conductivities, and the length of the structure as well as the axial strain can be employed as an effective way to tune their thermal conductivity.

Methods

To assess the thermal conductivity of 2D SWNT architecture, a series of reverse non-equilibrium molecular dynamics (RNEMD) simulations were performed by using the Large-scale Atomic/Molecular Massively Parallel Simulator (LAMMPS).[15] The idea of RNEMD is to divide the sample into several slabs along its length direction, and then exchanging the velocity of the hottest atom in the "cold" slab with the coldest atom in the "hot" slab.[16] This exchange scheme will generate an artificial heat flux to the sample and thus result in a temperature gradient as illustrated in Figure 1.

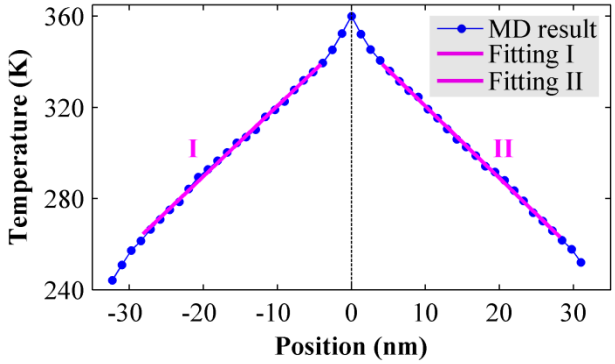

Figure 1 A stable temperature profile obtained from RNEMD simulation.

The heat flux J (in unit of Watt) that involves with a certain simulation time t can be calculated from, $J = 1/2tA\sum_{N}\frac{m}{2}(v_{hot}^2 - v_{cold}^2)$. Here A is the cross-sectional area, N is the total number of exchanges, m is the atomic mass, v_{hot} and v_{cold} are the velocities of the hot and cold atoms in the "cold" and "hot" slabs, respectively. The factor 2 in the denominator is used to account for the periodicity of the system. A steady state regime will arrive after certain exchanges, after which, the thermal conductivity (κ) can be calculated by following the Fourier's law, $\kappa = -J/(\partial T/\partial x)$. Here $\partial T/\partial x$ is the temperature gradient along the heat flux direction, which can be estimated from the temperature profile.

Different 2D SWNT architecture models have been considered, which are constructed from (6,6) SWNTs. The interactions between the bonded carbon atoms were described by the widely used adaptive intermolecular reactive empirical bond order (AIREBO) potential,[17] which has been shown to well represent the binding energy and elastic properties of carbon materials. A small time step of 0.5 fs was chosen. The initial equilibrium configuration of the sample was achieved by the conjugate gradient minimization method. Then the sample was equilibrated using Nose-Hoover thermostat[18, 19] under an ambient condition for 500 ps (temperature = 300 K and pressure = 1 atm). Finally, the system was switched to the microcanonical ensemble for 3 ns. Periodic boundary condition is only applied along the length direction.

Results and Discussion.

Structural influence. At the beginning, we investigate how the thermal conductivity will alter with different structures. Two types of 2D architectures have been constructed, i.e., hexagonal and orthogonal, which are generated by repeating Y-junctions and cross junctions in the two lateral directions, respectively (see Figure 2a and 2b). Specifically, the Y-junction is comprised by connecting three (6,6) SWNTs with an angle of 120° through either heptagons or octagons, and the cross junction is comprised by connecting four (6,6) SWNTs with an angle of 90° through a combination of pentagons, heptagons, and octagons.[11] To avoid the influence from geometry size, a similar size has been chosen for all models, $\sim 64 \times 10$ nm^2. The thickness of all models is determined by the diameter of the constituent (6,6) SWNT, which approximates to 0.9 nm.

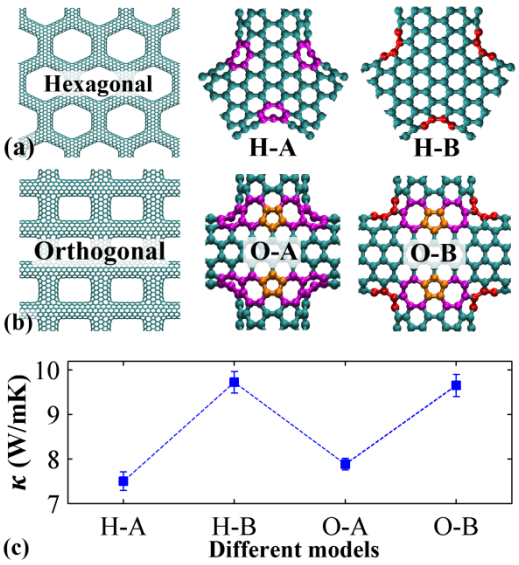

Figure 2 (a) The hexagonal 2D SWNT architecture constructed by Y-junctions; right shows two types of Y-junction connected by either heptagons (H-A) or octagons (H-B); (b) The orthogonal 2D SWNT architecture constructed by cross junctions; right shows two types of cross junction (O-A and O-B). The connecting pentagons, heptagons and octagons are highlighted by orange, magenta and red, respectively; (c) Thermal conductivity of different 2D SWNT architectures, the errorbar represents the standard deviation of the thermal conductivity during the simulation time of 1 to 3 ns.

In general, a relatively low thermal conductivity is estimated for different 2D SWNT architectures, e.g., κ for the H-A case is around 7.52 ± 0.21 W/mK. Such low thermal conductivity is majorly stemmed from the approximation of the cross-sectional area. For calculation simplicity, we adopted a simple continuum plate model to represent the complex porous and hollow SWNT architecture, which will overestimate the cross-sectional area. We should note that the so-called quantum corrections[20] can also be applied to improve the estimation of κ when the simulation is under the material's Debye temperature (~ 1000 K for nanotube[21]), while recent research found that quantum corrections in MD results above 200 K make marginal difference for κ when compared with the quantum predictions.[22] Therefore, following

discussions are emphasized on the relative value of the thermal conductivity, and quantum corrections are neglected in this work. According to Figure 2c, different junction types will result in different thermal conductivities and the nanoarchitecture with octagons (H-B and O-B) are found to have a larger thermal conductivity comparing with their counterparts without octagons. For instance, κ of H-B is around 30% larger than that of H-A.

To unveil the underneath mechanisms, we computed the vibrational density of states (VDOS) for the different 2D CNT-based structures, basing on the Fourier transformation of the autocorrelation function of the atomic velocities.[23] Considering that the heat is mostly carried by the in-plane longitudinal acoustic (LA), in-plane transverse acoustic (TA) phones, and out-of-plane acoustic (ZA) phonons, we decomposed the total VDOS into the in-plane and out-of-plane spectra by using the atomic velocity components in these corresponding directions. According to Figure 3a, the in-plane phonon modes of the architectures with octagons show higher peaks for both hexagonal and orthogonal structures. Similar results are also observed for the out-of-plane phonon modes as shown in Figure 3b. These observations explained that the 2D CNT-based structures which contain octagons possess higher thermal conductivity. Considering the ballistic nature of heat propagation in the architecture, the different thermal conductivities are originated from the different phonon scatterings at the junctions as indicated by the mismatches of the VDOS between the CNT and junction regions in Figure 3c and 3d. To note that the two orthogonal structures (O-A and O-B) shows much smaller amplitudes for the high-frequency phonon modes comparing with that of the hexagonal structures in Figure 3a. Whereas, the estimated κ does not follow such pattern, indicating certain inconsistencies with the Debye model for the specific heat of acoustic phonons,[24] i.e., smaller amplitudes

of the high-frequency phonon modes indicate smaller overall thermal conductivity. Such inconsistency is originated from the geometry size of different samples, which is not identical due to the nature of different junctions, while the sample sizes (along both lateral and longitudinal directions) exert significant impacts to the κ as discussed below.

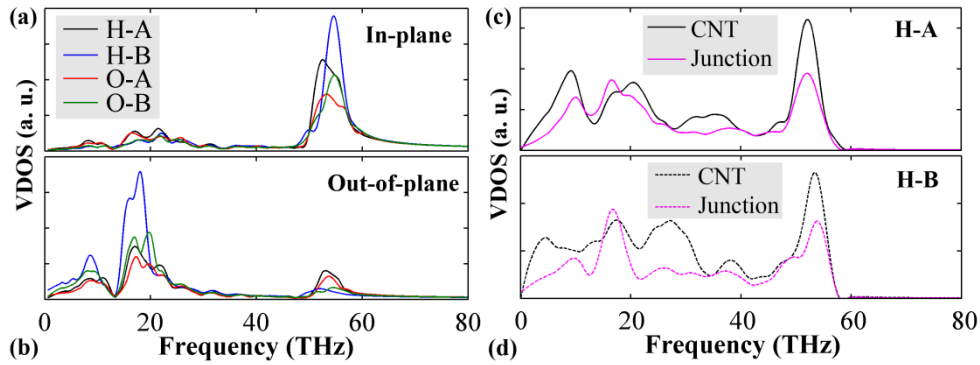

Figure 3 The VDOS of different structures for: (a) in-plane phonons; and (b) out-of-plane phonons; VDOS comparison between CNT and junction regions for: (c) sample H-A; and (d) sample H-B (the CNT and junction regions in a Y-junction unit has been selected for the VDOS computation).

Length dependence. We examine the length dependence of the thermal conductivity by considering the 2D SWNT architectures constructed by H-A Y-junction with an identical cross-sectional size of ~ 10×1 nm^2 and length ranging from 53 to 77 nm. As shown in Figure 4, a strong length dependent thermal conductivity is observed, the inverse of which exhibits a linear relation with the inverse of the sample length. Such phenomenon is in line with the common heuristic argument that when the periodic length of the simulation cell L is smaller than the phonon mean-free path Λ (Λ ~700-750 nm for SWNT at room temperature[1]), the inverse of thermal conductivity is proportional to the frequency of scattering events, with contributions from the sample ends and from intrinsic scattering,[25] i.e., $1/\kappa \propto 1/\Lambda + 1/L$. Apparently, by extrapolating the linear trend to L□□ (i.e., $1/L:\ 0$), the thermal conductivity will be

irrelevant or independent to the sample length L, approaching the limit thermal conductivity for a macroscopic 2D CNT nanoarchitecture κ_∞. From Figure 4, the limit of thermal conductivity for the 2D SWNT architecture (constructed by H-A Y-junction) is estimated as $\kappa_\infty = 8.5$ W/mK, i.e., κ will saturate to κ_∞ at 300 K while the sample size is much larger than the phonon mean-free path, changing from ballistic to diffusive phonon-transport regime.

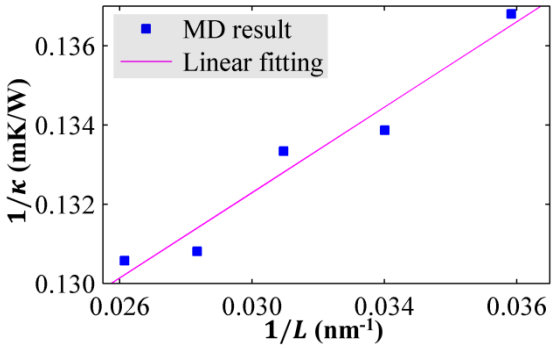

Figure 4 Thermal conductivity of the 2D SWNT architecture as a function of length.

Strain impacts. Further, we investigate the strain influence on the κ of the 2D SWNT architectures. A constant strain rate of 0.2 ns^{-1} was applied to the structure to achieve different strain values. Here the strain is defined as $\varepsilon = (L - L_0)/L_0$ (L_0 and L representing the initial and deformed length of the structure, respectively), and the atomic stress is computed basing on Virial stress.[26] It is worthy to mention that when the C-C bonds are stretched beyond 1.7 Å, a 1.7 Å cutoff distance for the AIREBO potential would lead to spuriously high tensile force. As suggested by previous researchers, a 2.0 Å cutoff can be chosen to overcome such abnormal phenomenon.[27] Though such phenomenon is also observed in the 2D CNT-based structures, our simulations reveal that the change of cutoff distance from 1.7 Å to 2.0 Å exert marginal influence to the elastic deformation of the structure ($\varepsilon <$ ~ 9.5%, see Figure 5a). As expected, the constituent CNTs of the H-A architecture are compressed along

the lateral direction while stretched along the length direction due to the tensile loading, reflecting the possion's ratio of the structure (refer to left inset of Figure 5a). Specifically, all C-C bonds around the stretched region are smaller than the initial 1.7 Å cutoff distance at the strain of 9% (see right inset of Figure 5a). Therefore, a cutoff distance of 1.7 Å is chosen for the tensile deformation to achieve a pre-strained structure for discussion consistency.

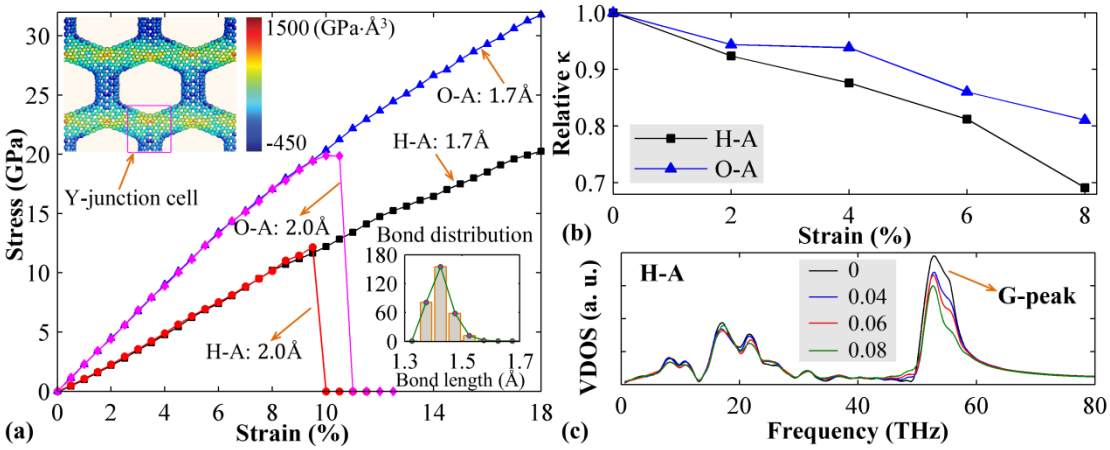

Figure 5 (a) Stress-strain curve of the 2D SWNT architectures made from H-A & O-A junctions, left inset shows the atomic stress (in the unit of GPa·Å^3) distribution in the H-A architecture at 9% strain, right inset shows the corresponding bond length distribution for a Y-junction cell; (b) The relative thermal conductivities of H-A & O-A architectures as a function of strain; (c) The total VDOS of H-A architecture under the axial strain of 0, 0.04, 0.06 and 0.08.

Figure 5b shows that the thermal conductivities of the 2D SWNT architectures decrease monotonically with increasing axial strain. For instance, a 8% axial strain is found to induce ~ 30% (~ 20%) reduction to the κ of H-A (H-B) structure. Such observations are in line with the results reported for CNT[28] and graphene nano-ribbon.[29] According to the kinetic theory, the thermal conductivity of a solid can be expressed as $\kappa = \sum_\lambda C_\lambda \upsilon_\lambda \Lambda_\lambda$, where λ is the phonon mode index. C and υ are the

specific heat and group velocity of each phonon mode, respectively. The existence of axial tensile strain will soften the high-frequency phonon modes (i.e., the G-peak, see Figure 5c), which decreases specific heat and thus lead to a reduction to κ.[30] Interestingly, Figure 5b suggests that the axial strain induces larger reduction to κ for the H-A structure with a lower Young's modulus (as seen in the stress-strain curve in Figure 5a). It can be concluded that the thermal transport properties of the 2D CNT-based structures can be effectively tailored through the modulation of axial strain.

Conclusions

In summary, basing on large-scale nonequilibrium molecular dynamics simulations, the thermal conductivity of 2D SWNT-based structures has been studied. Under high temperature, the feasibility of welding SWNTs into network structures by electron beam suggests an appealing way for the thermal properties engineering for carbon-based nanoarchitectures. It is found that the length of the architecture as well the axial strain can be employed as an effective way to tune its corresponding thermal conductivity. For instance, a 8% axial strain can induce ~30% reduction to the thermal conductivity of the 2D SWNT architecture. This study sheds lights on the nanoscale thermal/phonon engineering by utilizing SWNTs.

Acknowledgments

Supports from the ARC Discovery Project (DP130102120) and the High Performance Computer resources provided by the Queensland University of Technology are gratefully acknowledged. Dr Zhan is grateful to Dr Zhou from Hefei University of Technology (China) for providing the advices in constructing the models.

References

1. A. A. Balandin, Nat. Mater. **10** (8), 569-581 (2011).
2. D. L. Nika, A. S. Askerov and A. A. Balandin, Nano Lett. **12** (6), 3238-3244 (2012).
3. J. Hu, X. Ruan and Y. P. Chen, Nano Lett. **9** (7), 2730-2735 (2009).
4. H. Zhan, Y. Zhang, J. M. Bell, Y.-W. Mai and Y. Gu, Carbon **77**, 416-423 (2014).
5. Q. X. Pei, Y. W. Zhang, Z. D. Sha and V. B. Shenoy, Appl. Phys. Lett. **100** (10), 101901 (2012).
6. Y. Zhu, L. Li, C. Zhang, G. Casillas, Z. Sun, Z. Yan, G. Ruan, Z. Peng, A.-R. O. Raji and C. Kittrell, Nat. Commun. **3**, 1225 (2012).
7. V. Varshney, S. S. Patnaik, A. K. Roy, G. Froudakis and B. L. Farmer, ACS Nano **4** (2), 1153-1161 (2010).
8. M. Terrones, Annu. Rev. Mater. Res. **33** (1), 419-501 (2003).
9. L. P. Biró, Z. E. Horváth, G. I. Márk, Z. Osváth, A. A. Koós, A. M. Benito, W. Maser and P. Lambin, Diamond Relat. Mater. **13** (2), 241-249 (2004).
10. V. R. Coluci, D. S. Galvao and A. Jorio, Nanotechnology **17** (3), 617 (2006).
11. R. Zhou, R. Liu, L. Li, X. Wu and X. C. Zeng, J. Phys. Chem. C **115** (37), 18174-18185 (2011).
12. L. Ying, Q. XinMing, Y. Fan, W. Xi-Shu, Y. Yajun and F. Qinshan, J. Phys. D: Appl. Phys. **41** (15), 155423 (2008).
13. Z. Qin, X.-Q. Feng, J. Zou, Y. Yin and S.-W. Yu, Appl. Phys. Lett. **91** (4), 043108 (2007).
14. M. P. Nicola, Nanotechnology **17** (21), 5480 (2006).
15. S. Plimpton, J. Comput. Phys. **117** (1), 1-19 (1995).
16. F. Muller-Plathe, J. Chem. Phys. **106** (14), 6082-6085 (1997).
17. D. W. Brenner, O. A. Shenderova, J. A. Harrison, S. J. Stuart, B. Ni and S. B. Sinnott, J. Phys.: Condens. Matter **14** (4), 783 (2002).
18. W. G. Hoover, Phys. Rev. A **31** (3), 1695-1697 (1985).
19. S. Nosé, J. Chem. Phys. **81**, 511 (1984).
20. C. Wang, C. Chan and K. Ho, Phys. Rev. B **42** (17), 11276 (1990).
21. T. Tohei, A. Kuwabara, F. Oba and I. Tanaka, Phys. Rev. B **73** (6), 064304 (2006).
22. J. Turney, A. McGaughey and C. Amon, Phys. Rev. B **79** (22), 224305 (2009).
23. J. Dickey and A. Paskin, Phys. Rev. **188** (3), 1407 (1969).
24. E. Pop, V. Varshney and A. K. Roy, MRS Bull. **37** (12), 1273-1281 (2012).
25. P. K. Schelling, S. R. Phillpot and P. Keblinski, Phys. Rev. B **65** (14), 144306 (2002).
26. J. Diao, K. Gall and M. L. Dunn, J. Mech. Phys. Solids **52** (9), 1935-1962 (2004).
27. O. A. Shenderova, D. W. Brenner, A. Omeltchenko, X. Su and L. H. Yang, Phys. Rev. B **61** (6), 3877-3888 (2000).
28. X. Zhiping and J. B. Markus, Nanotechnology **20** (18), 185701 (2009).
29. W. Ning, X. Lanqing, W. Hui-Qiong and Z. Jin-Cheng, Nanotechnology **22** (10), 105705 (2011).
30. J. Chen, J. H. Walther and P. Koumoutsakos, Nano Lett. **14**, 819-825 (2014).